



Spatiotemporal changes and driving factors of vegetation in 14 different climatic regions in the global from 1981 to 2018

Guangchao Li¹ · Wei Chen¹ · Xuepeng Zhang¹ · Zhen Yang² · Zhe Wang¹ · Pengshuai Bi¹

Received: 18 February 2022 / Accepted: 23 May 2022 / Published online: 2 June 2022
© The Author(s), under exclusive licence to Springer-Verlag GmbH Germany, part of Springer Nature 2022

Abstract

Climate change affects the change of vegetation, and the analysis of vegetation change and its drivers in different globe climate zones is important for ecological conservation, energy balances, and climate change in different global climate zones. Based on the vegetation leaf area index (LAI) and climate factor datasets, this paper uses an integrated empirical model decomposition, sensitivity rate, contribution rate, and geographic detector analysis method to study the vegetation drivers and their changes in 14 different climate zones around the globe from 1981 to 2018. The results showed that (1) Vegetation changes were sensitive to precipitation and evapotranspiration in arid climate zones and to temperature and soil temperature in cold climate zones. In the tundra climate zone, the sensitivity of vegetation change to temperature was higher than that to precipitation and evapotranspiration. (2) Soil moisture has the highest contribution to vegetation change, and the areas with absolute contribution rates over 60% account for 50.26% of the total area of global vegetation cover. The areas with high contributions of temperature and soil temperature to the LAI are mainly distributed in the Northern Hemisphere, which indicates that temperature has a high contribution to vegetation change in low-temperature environments. (3) The areas with significant increasing trends for the global vegetation LAIs accounted for approximately 15.32% of the total global vegetation cover (slope ≥ 0.01), which are mainly located in equatorial savannahs with dry winters, warm temperate climates with dry winters, and warm temperate climates with fully humid climatic zones. (4) The LAIs were dominated by medium-high fluctuations and sustainable increasing changes, which accounted for 61.27% and 69.34% of the total global vegetation cover area, respectively. (5) Globally, the driving factors influencing LAI changes are specific humidity, temperature, soil temperature, evapotranspiration, precipitation, and soil moisture in descending order, with the largest interaction effect of specific humidity and soil moisture on LAI changes. This research provides a scientific basis for vegetation change monitoring, driving mechanisms, and ecological protection in different climate regions around the globe.

Keywords Vegetation change · Leaf area index · Climate change · Sensitivity · Contribution

Introduction

Global greening affects climate change and the carbon cycle, which in turn affects land-based ecosystem functions and services (Chen et al. 2019; Zhu et al. 2016). Vegetation influences the carbon balance of terrestrial ecosystems

through photosynthesis and respiration and regulates climate change in different regions of the globe (Jin et al. 2017; Zhang and Chen 2021). With the large-scale monitoring of vegetation change emerging as a hot spot for scientific research, the global high spatiotemporal resolution vegetation index remote sensing products have become a technical means to monitor global vegetation changes (Sprintsin et al. 2007; Zhu et al. 2014). Various remote sensing products already exist for monitoring vegetation change at large scales and over long time series, such as the normalized difference vegetation index (NDVI) and leaf area index (LAI) (Gao et al. 2019; Liu et al. 2018).

LAI remote sensing products can accurately monitor dynamic changes in vegetation. At present, global LAI datasets at different scales already exist, for example, global LAI

Responsible Editor: Diane Purchase

✉ Wei Chen
chenw@cumtb.edu.cn

¹ College of Geoscience and Surveying Engineering, China University of Mining & Technology, Beijing 100083, China

² College of Information Science and Engineering, Henan University of Technology, Zhengzhou 450001, China

datasets at 1 km, 0.05°, and 1/12 degree resolution (Kahiu and Hanan 2018; Pascolini-Campbell et al. 2021; Xiao et al. 2014; Xiao et al. 2016). The LAI represents the key parameters of vegetation photosynthesis areas and canopy structures, which directly affect the levels of solar radiation absorption, photosynthesis, and energy exchange of plants (Chen et al. 2016; Ge et al. 2019; Hu et al. 2021; Zhu et al. 2014). Meanwhile, the LAI is also the main input parameter for models such as those for Earth system processes and terrestrial biospheres (Liu et al. 2012). Therefore, analyzing the spatiotemporal variation of LAI and its driving factors in different climate zones around the globe is essential for the long-term improvement of global vegetation change monitoring and ecosystem protection. Many researchers have used the above-mentioned remote sensing dataset to monitor the spatiotemporal dynamics of vegetation in long-term series. For example, some scholars have used linear methods to study the spatiotemporal changes of vegetation LAI (Chen et al. 2020; Liu et al. 2010; Piao et al. 2015). In addition, some scholars have used the ensemble empirical mode decomposition (EEMD) method to study the nonlinear spatiotemporal variations in vegetation (Liu et al. 2018; Yin et al. 2017). Although the above studies can express the spatiotemporal trend of LAI in the entire study area, it does not involve the analysis of changes in LAI in different climatic regions and the analysis of the stability and sustainability of LAI in different climatic regions.

Vegetation growth is dominated by temperature, precipitation, and radiation (Guli-Jiapaer et al. 2015, Li et al. 2019, Liang et al. 2020). Evapotranspiration is very important in the global hydrological water cycle and energy balance and is an important component of ecological hydrological processes (Birhanu et al. 2019; Niu et al. 2019). As determined by satellite remote sensing monitoring, the vegetation LAIs are increasing, and the main causes of global greening may be climate change and CO₂ fertilization effects (Chen et al. 2019). However, global greening slows down the rate of increase in global land surface air temperatures, which leads to increases in evapotranspiration and negative combined warming values (Zeng et al. 2017). Xiao and Moody (2004) studied the correlation between the LAI and temperature in China based on LAI and climate datasets from 1982 to 1998 and showed that temperature is the dominant factor that determines the spatial distribution of greening in China. Zhu et al. (2016) studied the driving factors of the LAI from 1982 to 2009 and showed that the impact of carbon dioxide on vegetation change was the highest among the four driving factors. Moreover, several scholars have studied the interactions between vegetation and drought, and between vegetation and water use efficiency (Deng et al. 2021; Hu et al. 2008; Li et al. 2018; Zhang et al. 2018).

The innovation of this paper lies in a more detailed analysis of the changing trends, stability, and sustainability

of vegetation in different climate zones around the world from 1981 to 2018. Meanwhile, the sensitivity rate of vegetation change to climatic factors and the contribution rate of climatic factors to vegetation change in different climatic regions were comprehensively analyzed. The main research objectives are (1) to compare the global linear and nonlinear spatiotemporal change trends in vegetation cover and the spatiotemporal distributions of vegetation cover nonlinear change types from 1981 to 2018; (2) analyze the spatial distribution characteristics of the stability and sustainability of global vegetation and the change trends of vegetation in different ecosystems; (3) study the geographic distributions of the sensitivity rates of global vegetation change to six driving factors; and (4) analyze the geographic distributions of the contribution rates of the six driving factors to vegetation change in different global climate regions. This research helps us understand the role of long-term vegetation change and its climate-driving mechanism in global change.

Data and methods

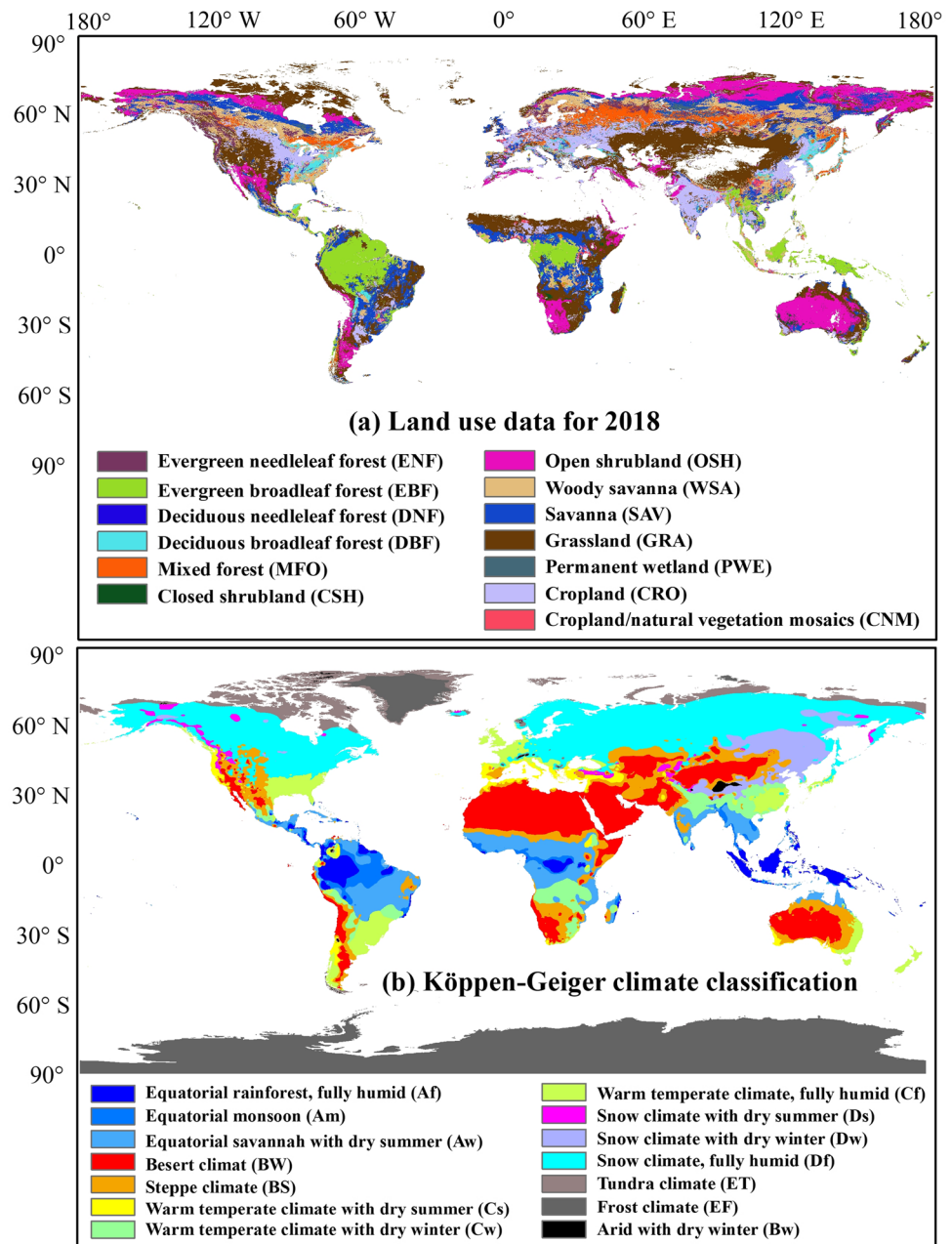
Data

We selected vegetation LAI product data with monthly and 0.05° resolutions, and the time range was 1981–2018 (Xiao et al. 2014). The driving factor dataset used in this paper is provided by the Famine Early Warning Systems Network Land Data Assimilation System Products and includes evapotranspiration (Evap), temperature (Temp), precipitation (Pre), specific humidity (Qair), soil moisture (SoilMoi), and soil temperature (SoilTemp) data. This data product covers the period from 1982 to 2018, with a spatial resolution of 0.1° (McNally et al. 2017). This paper selects the 2001–2018 land use data (MCD12C1) with a resolution of 0.05°, including 17 land use types. Only the areas covered by 13 vegetation types are studied in this paper, and the full names and abbreviations of these 13 land use types in 2018 are shown in Fig. 1a. This paper adopts the Köppen-Geiger global climate classification (GCC) data (Kottek et al. 2006), which includes 14 climate zones. The full names and abbreviations of these climate zones are shown in Fig. 1b.

Methods

Based on the global LAI and driver datasets, this paper studies vegetation drivers and their changes in 14 different climate zones around the world from 1981 to 2018. The overall technical process is shown in Fig. 2.

Fig. 1 Spatial distributions of global land use types and climate classifications, (a) Land use data for 2018, (b) Köppen-Geiger climate classification



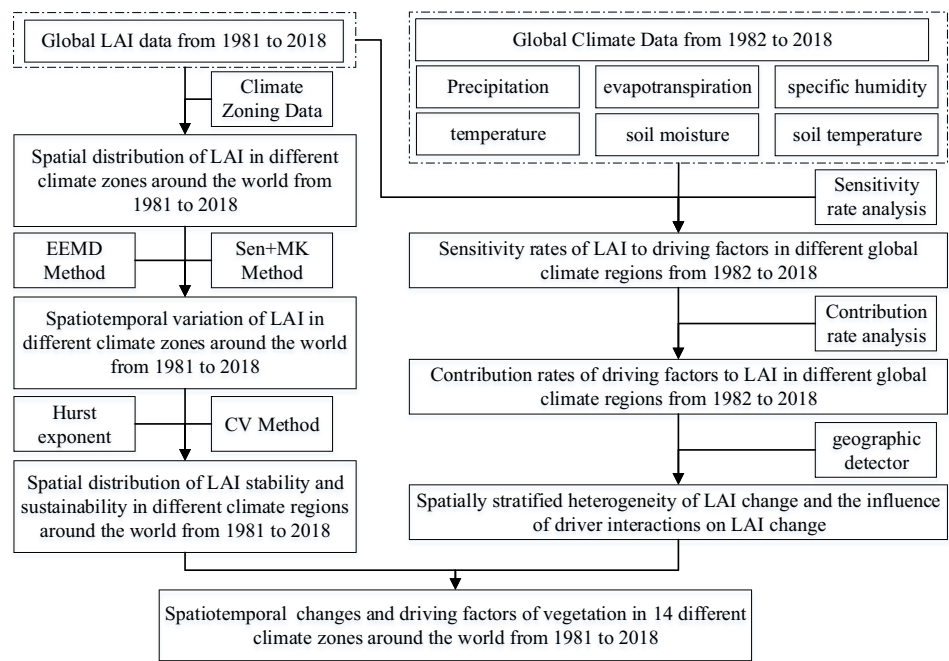
Trend analysis

This article uses linear and nonlinear trend analysis methods to analyze the global vegetation LAI change trends, and the linear trend analyses use the Theil-Sen median method (Liu et al. 2015). For the detailed calculation formulas, please refer to the literature of Li et al. (2021). The nonlinear trend analysis method uses the EEMD method, which can be used to capture the nonlinear elements of statistical trends. This method is an improvement of the traditional empirical mode decomposition (EMD) method. By adding different levels of Gaussian white noise to the original signal multiple times

and then conducting multiple EMDs on the composite signal, multiple groups of intrinsic mode functions (IMFs) are obtained, and the average value is used as the final IMF (Zhang et al. 2016). The EMD method assumes that any signal is composed of a finite number of eigenmode functions, and the signal is decomposed into a more easily analyzed set of several eigenmode functions and a set of residuals with full adaptivity by EMD (Huang et al. 1998). The EEMD calculation steps are as follows:

Gaussian white noise $w(t)$ of equal length and unequal amplitude is added to the original signal $x(t)$ to obtain a new signal $X(t)$ to be decomposed:

Fig. 2 Overall technical flow-chart



$$X(t) = x(t) + w(t) \tag{1}$$

Firstly, the curve transformation of the time series signal with white noise is carried out, the local maximum and minimum values of the frequency band signal are extracted, and the extreme point is interpolated by the cubic spline. Then, all the local maximum and minimum points are linked by a curve to form the upper envelope ($ue(t)$) and lower envelope ($le(t)$) respectively and calculate the average value $\varphi_1(t) = \frac{ue(t)+le(t)}{2}$ of $ue(t)$ and $le(t)$. Finally, subtract $\varphi_1(t)$ from $X(t)$:

$$X_1(t) = X(t) - \varphi_1(t) \tag{2}$$

Determine whether the above process can continue based on the standard deviation (SD):

$$SD = \sum_{i=0}^t \left[\left| X_1(t) - X_{(i-1)}(t) \right|^2 / X_{(i-1)}^2(t) \right] \tag{3}$$

The i in formula (3) is the number of iterations. If the SD is less than a preset threshold value, the above calculation process is stopped and the first IMF1 is calculated:

$$IMF1 = X_j(t) = X_{j-1}(t) - \varphi_j(t) \tag{4}$$

The residuals of the signal $X_1(t)$ and IMF1 are calculated:

$$R(t) = X_1(t) - IMF1 \tag{5}$$

Repeat formula (1) and formula (5) until $R_n(t)$ becomes a monotonic function:

$$R_i = R_{i-1} - IMF_i, i = 2, 3, \dots, n \tag{6}$$

Based on the above steps, the number of residuals and IMFs separated by $x(t)$ is obtained.

$$x(t) = \sum_{i=1}^n IMF_i(t) + R(t) \tag{7}$$

Coefficient of variation

The coefficient of variation (CV) is used to quantitatively characterize the degree of interannual variation in the LAI:

$$CV_{LAI} = \frac{\sigma_{LAI}}{LAI} \tag{8}$$

where CV_{LAI} represents the coefficient of variation for each pixel of the global LAI from 1981–2018, σ_{LAI} is the standard deviation of the LAI values, and LAI is the multi-year average of the global LAI values from 1981 to 2018. In this study, CV_{LAI} was divided into five levels: high fluctuation ($CV_{LAI} > 0.5$), medium-high fluctuation ($0.15 < CV_{LAI} < 0.5$), medium fluctuation ($0.1 < CV_{LAI} < 0.15$), medium-low fluctuation ($0.05 < CV_{LAI} < 0.1$), and low fluctuation ($CV_{LAI} < 0.05$).

Hurst exponent

A rescaled polar difference (R/S) analysis-based approach was used to calculate the Hurst exponent to characterize the interannual sustainability of the LAI. Sustainability is the

constraint of the resource system on human beings to meet their needs, and its internal dynamic mechanism lies in the unity of the resource system's internal sustainability and external support and regulation capabilities, as well as the synergy of various internal and external structures, functions, and benefits. The purpose of calculating the sustainability of global vegetation is to analyze the spatiotemporal distribution of the sustainable utilization of global vegetation resources. The formula is shown as follows.

Let the LAI time series $\{LAI_i\}$, $i = 1, 2, \dots, n$, for any positive integer, m , define the time series:

$$\Delta LAI_i = LAI_i - LAI_{i-1} \quad (9)$$

Assume that the mean series of the time series is

$$\left\{ \overline{LAI}_{(t)} \right\} = \frac{1}{\tau} \sum_{i=1}^{\tau} LAI_{(i)}, \tau = 1, 2, \dots, n \quad (10)$$

The cumulative deviations are

$$X_{(i,\tau)} = \sum_{i=1}^i \left(LAI_{(i)} - \overline{LAI}_{(i)} \right), 1 \leq i \leq \tau \quad (11)$$

Calculate the range of the cumulative deviations:

$$R_{(\tau)} = \max_{1 \leq i \leq \tau} X_{(i,\tau)} - \min_{1 \leq i \leq \tau} X_{(i,\tau)}, \tau = 1, 2, \dots, n \quad (12)$$

Calculate the standard deviation:

$$S_{(\tau)} = \left[\frac{1}{\tau} \sum_{i=1}^{\tau} \left(LAI_{(i)} - \overline{LAI}_{(i)} \right)^2 \right]^{1/2}, \tau = 1, 2, \dots, n \quad (13)$$

Hurst index calculation:

$$\frac{R_{(\tau)}}{S_{(\tau)}} = (\tau)^H \quad (14)$$

Both sides of formula (14) were taken logarithmically and were then linearly fitted using least squares to find the H value. In this study, the Hurst index is divided into three types. For the details, refer to Fig. 7.

Sensitivity and contribution rates

The sensitivity rate (SR) of the vegetation LAI to the driving factors was defined as (Sun et al. 2021; Zheng et al. 2009):

$$SR = \frac{\overline{DF}}{\overline{LAI}} * \frac{\sum (DF_i - \overline{DF})(LAI_i - \overline{LAI})}{\sum (DF_i - \overline{DF})} \quad (15)$$

where DF_i is the annual average value of the driving factors in year i , including Evap, Temp, Pre, Qair, SoilMoi, and SoilTemp. LAI_i denotes the LAI in year i . \overline{DF} and \overline{LAI} are

the mean values of the driving factors and LAIs from 1982 to 2018, respectively.

The contribution rate (CR) of the driving factors to the vegetation LAI is defined as (Sun et al. 2021; Yin et al. 2010):

$$CR = \frac{\Delta DF}{DF} \times SR \times 100\% \quad (16)$$

In the formula, ΔDF represents the relative change in the impact factors. CR describes the relative contributions of the impact factors. ΔDF is defined as

$$\Delta DF = \frac{37 \times Sen_{slope}}{|av|} \times 100\% \quad (17)$$

In the formula, Sen_{slope} represents the rate of change of the impact factor over 37 years, and $|av|$ represents the absolute average of the impact factor. In this paper, formulas (15–17) are used to calculate the sensitivity rate of vegetation LAI to driving factors and the contribution rate of driving factors to LAI.

Geographical detector

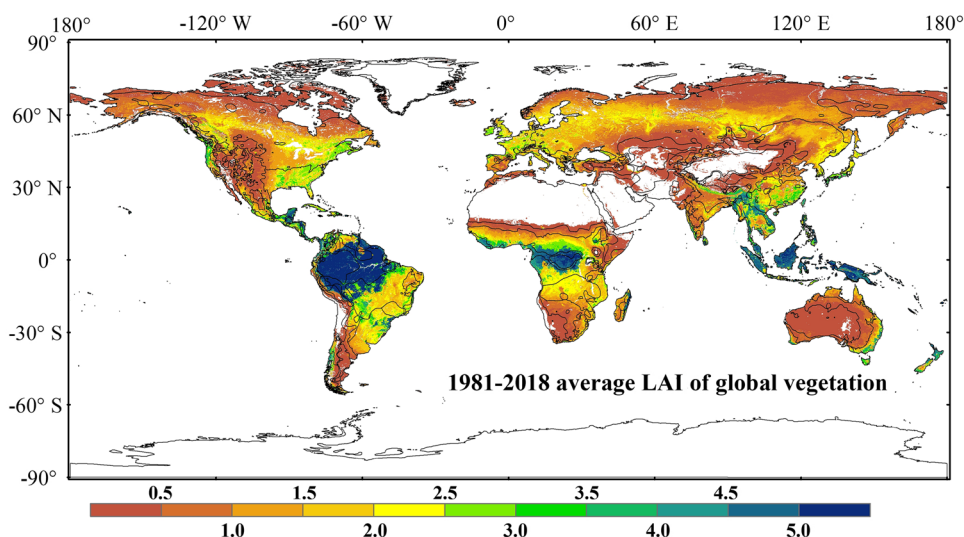
Geographical detector is a new statistical method for detecting spatial differentiation and revealing the driving factors behind it, which is free of linear assumptions and has an elegant form and a clear physical meaning. The technique is based on the theory of spatial differentiation, aggregation, and overlap to analyze the consistency of the independent and dependent variables in the geographic layer space and is able to quantify the effect of one or more independent variables on the dependent variable. The basic idea and principle of the geographical detector can be found in Wang et al. (2016). In this paper, we use geographical detector to study the effects of Evap, Temp, Pre, Qair, SoilMoi, and SoilTemp on vegetation change globally and in different climate zones, and we calculate the characterization indicators of vegetation LAI growth change based on the Sen Median method and use the geographical detector algorithm to study the effects of drivers on LAI change trends globally and in different climate zones. The \cap symbol represents the effect of the interaction of two independent variables on the dependent variable, for example, $Qair \cap SoilMoi$ represents the effect of the interaction of Qair and SoilMoi on the change in LAI.

Results

Average LAI of global vegetation

Spatial distribution of the average value of global vegetation LAI from 1981 to 2018 is shown in Fig. 3. The regions

Fig. 3 Spatial distribution of the average values of the global vegetation LAI from 1981 to 2018



with high LAI multiyear average values (≥ 4) are concentrated in Af and Am climatic zones whose areas account for 8.91% of the total area of global vegetation coverage. This phenomenon is related to adequate climatic conditions such as temperature, precipitation, and light in Af and Am climatic regions. The regions with low LAI multiyear average values (< 2) are concentrated in the BW, BS, and Df climatic zones, which account for 75.95% of the total area of global vegetation coverage. This phenomenon is related to the insufficient precipitation for tree growth in the BW and BS climatic zones, and to the fact that the subsurface of the Df climatic zone is covered by snow and ice all year round.

Global spatiotemporal vegetation changes

Global vegetation spatial change

Based on the EEMD method, the global LAI annual mean value nonlinear spatial change trends and statistics from 1981 to 2018 were analyzed (Fig. 4a). The areas of the global vegetation LAI that showed increasing trends accounted for approximately 33.24% of the total area of global vegetation coverage (slope ≥ 0.005). Among them, the areas showing significant growth trends account for approximately 15.32% of the total area of global vegetation coverage (slope ≥ 0.01) and are mainly distributed in the Aw, Cw, and Cf climatic zones. The areas where the global vegetation LAI shows decreasing trends account for approximately 13.46% of the total area of global vegetation coverage (slope ≤ -0.005). Among them, the areas with significant decreasing trends account for approximately 6.53% of the total area of global vegetation coverage (slope ≤ -0.01), which are scattered around the world. The areas with insignificant change trends in the global vegetation LAI account for approximately 53.31% of the

total area of global vegetation coverage ($-0.005 < \text{slope} < 0.005$) and are mainly distributed in the Df, BW, and BS climatic zones. Based on the Sen and EEMD methods, the results of analyzing the spatial distribution of the global vegetation LAI annual mean value change trend are generally consistent (Fig. 4b). However, the area proportions of the significant change trends of the global vegetation LAI that were analyzed by the Sen method are less than those determined by the EEMD method. For example, the significant change trend area of the global vegetation LAI from 1981 to 2018 accounted for approximately 17.17% (less than 21.58%) of the total area of global vegetation coverage. In contrast, the area proportion of the global vegetation LAI with insignificant change trends was higher than that determined by the EEMD method.

Fig. 5 shows the spatial distributions and statistics of the nonlinear spatial change trend types of the global vegetation LAI from 1981 to 2018. As seen from the figure, the global vegetation LAI is dominated by a trend of increasing and then decreasing, which occurs for approximately 38.61% of the total area of global vegetation cover, and this trend is distributed throughout the global vegetation coverage area. This is followed by a decreasing and then increasing change trend, which accounts for approximately 31.60% of the total area of global vegetation cover and is concentrated in south-central North America, southern South America, southern Africa, southeast Asia, and central and northern Australia. In addition, the proportion of the areas with monotonic change trends in the global vegetation LAI is relatively small, and the areas with monotonically increasing change trends and monotonically decreasing change trends account for 22.63% and 7.16% of the total area covered by global vegetation, respectively. Among them, the regions with monotonically increasing trends of the vegetation LAI were distributed in south-central North America, northern South America,

Fig. 4 Nonlinear and linear spatial variation trends and statistics of the global LAI annual mean values from 1981 to 2018, (a) 1981-2018 EEMD trend, (b) 1981-2018 Sen trend

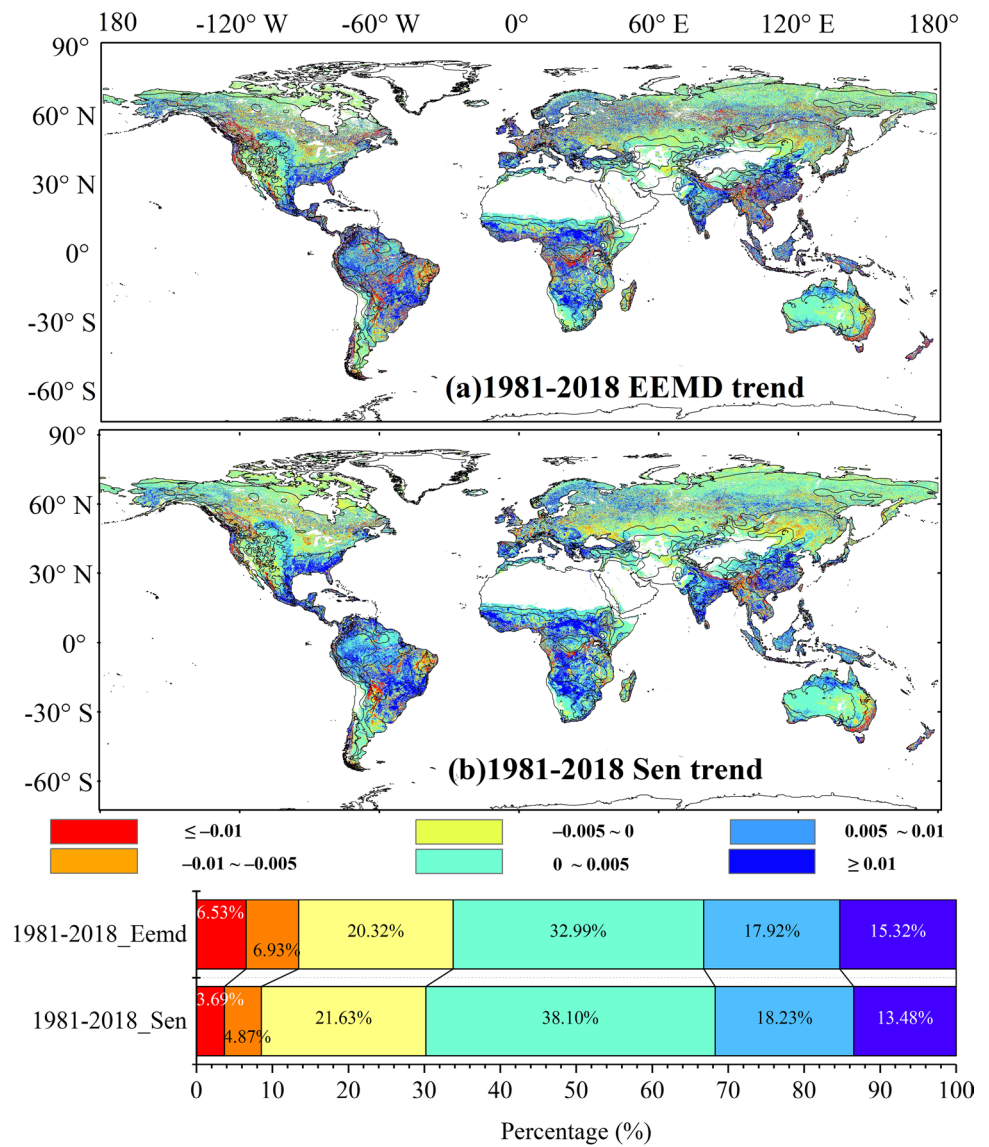
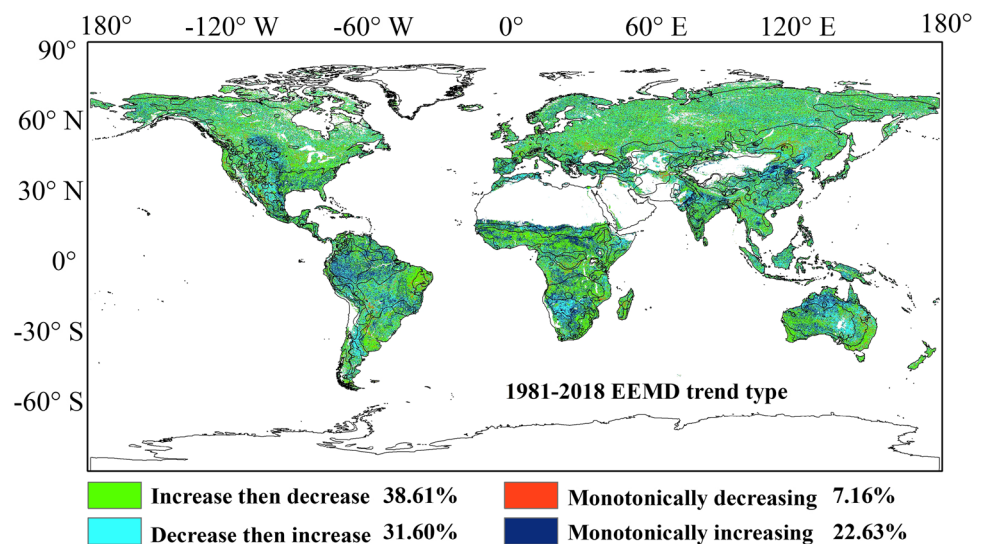


Fig. 5 Distributions and statistics of nonlinear spatial change trend types of the global LAI annual mean values from 1981 to 2018



central and southern Africa, southeastern and southwestern Asia, and northern Australia.

Temporal change trends of global vegetation

Fig. 6 shows the linear and nonlinear change trends of the annual average global vegetation LAIs from 1981 to 2018, which indicates that the global vegetation LAIs exhibited an increasing trend from 1981 to 2018. Among them, the linear change trend ($2.88 \times 10^{-3} \text{ year}^{-1}$) is greater than the nonlinear change trend ($1.91 \times 10^{-3} \text{ year}^{-1}$). The results of the nonlinear method show that the annual average values of the global vegetation LAIs showed a change trend of first increasing and then decreasing from 1981 to 2018. The global vegetation LAI multiyear average was 1.4307 and reached a maximum in 2000, while the annual average LAIs fluctuated from 1.3239 to 1.5024.

Variation trends of LAI in different ecosystems

Fig. 7 shows the change trends and box diagrams of the vegetation LAI in different ecosystems around the world from 2001 to 2018. Evergreen broadleaf forests have the highest multiyear average LAIs (4.7), and open shrubs have the lowest multiyear average LAIs (0.38). Except for the evergreen needleleaf forests, evergreen broadleaf forests, cropland/natural vegetation mosaics, and closed shrubland types, the LAIs for the other vegetation types all exhibit increasing trends. Among them, permanent wetlands have the highest growth rate, and grasslands have the lowest growth rate. The annual average LAI values in different ecosystems from large to small are EBF > DBF > MFO > ENF > WSA > SAV > DNF > CNM > CRO > PWE > CSH > GRA > OSH.

Fig. 6 Linear change trends (a) and nonlinear change trends (b) of the annual average values of the global vegetation LAI from 1981 to 2018

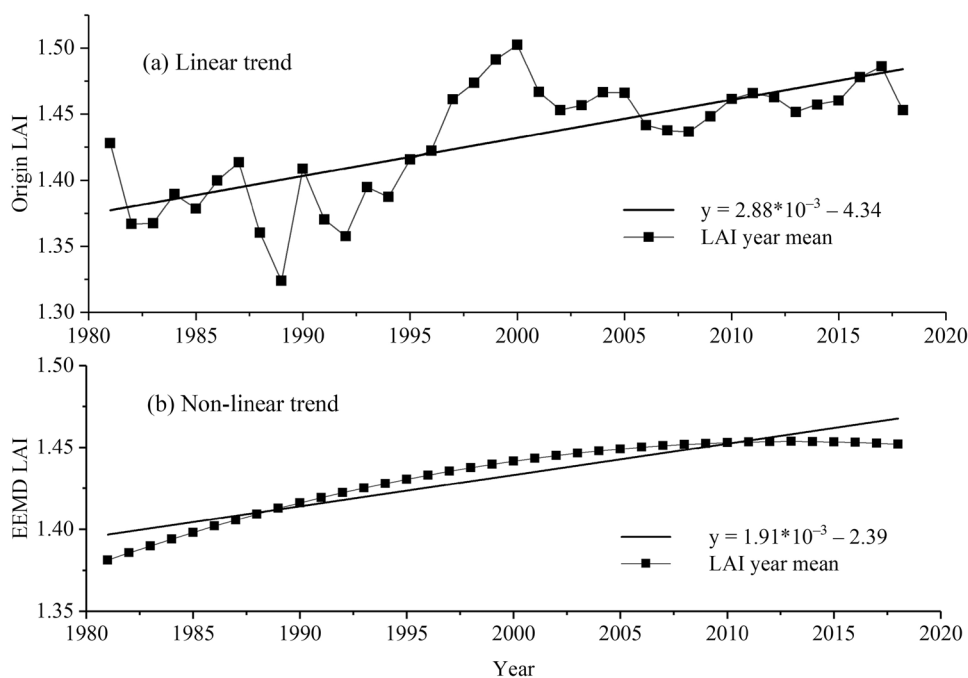
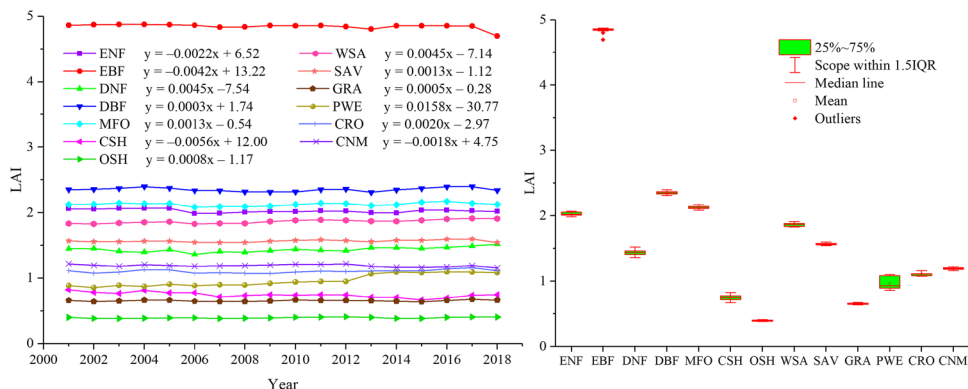


Fig. 7 2001–2018 global vegetation change trends and box diagrams in different ecosystems



Stability and sustainability of global vegetation

The spatial distributions of the coefficients of variation of the global vegetation LAI from 1981 to 2018 are shown in Fig. 8, and the mean value of the coefficients of variation of the LAI is 0.25. The areas with high LAI fluctuations account for approximately 6.88% of the total area covered by global vegetation, which is concentrated in the ET climate zone, and the rest of the areas are scattered. The areas with medium-high LAI fluctuations accounted for approximately 61.27% of the total area of global vegetation cover and were mainly distributed in the Df, BW, and BS climatic zones. The areas with medium LAI fluctuations accounted for approximately 17.07% of the total area of global vegetation cover and were concentrated in the Aw and Cw climate zones. The areas of medium-low fluctuations and low LAI fluctuations accounted for approximately 14.78% of the total area of global vegetation cover and were located mainly in

the Af and Am climatic zones. The spatial distribution of the coefficients of variation of the global LAI is very similar to the spatial distribution of the LAI multiyear mean, and the higher the LAI value is, the lower the fluctuation is.

The spatial distribution of the global vegetation LAI Hurst index from 1981 to 2018 is shown in Fig. 9. The sustainable increase area in the global vegetation LAI accounted for 69.34% of the total area of global vegetation coverage. Among them, the sustainable and significant increases in the vegetation LAI accounted for 34.65% of the total area of global vegetation coverage, which were mainly in the Af, Am, Aw, and Cw climatic zones. The sustainable decrease area of the vegetation LAI accounted for 27.75% of the total area of global vegetation coverage. Among them, the sustainable and significant reduction areas of the vegetation LAI accounted for 5.9% of the total area of global vegetation coverage, which mainly occurred in the Dw and Cf climate zones. In addition, the areas in which the trend

Fig. 8 The spatial distribution of global LAI fluctuations from 1981 to 2018

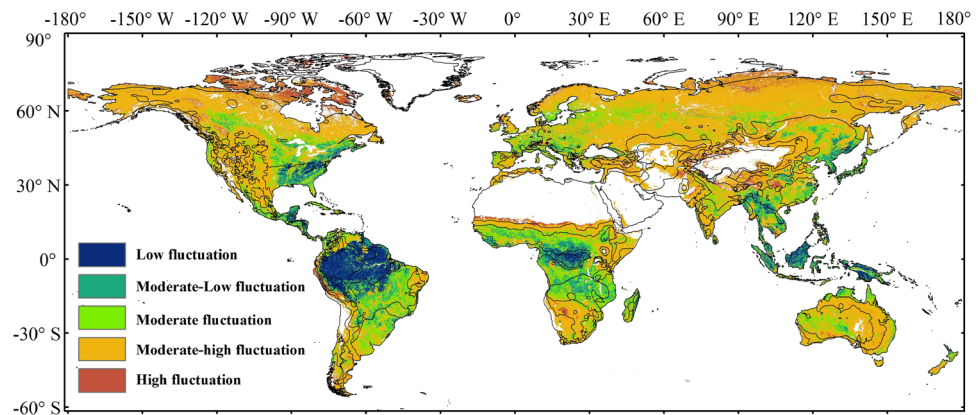
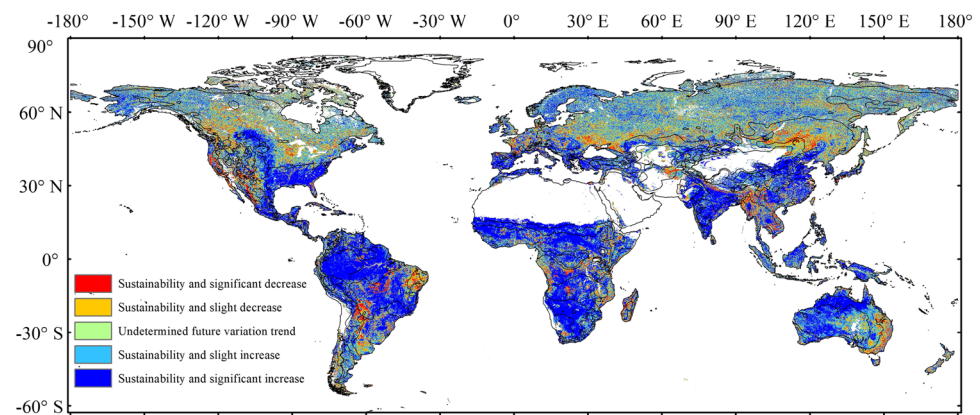


Fig. 9 The dynamic spatial distribution and statistics of the global LAI Hurst index from 1981 to 2018



β value	Z value	H value	LAI variation types	Area percentage/%
$\beta < 0$	$ Z \geq 1.96$	> 0.5	Sustainability and significant decrease	5.90
$\beta < 0$	$ Z < 1.96$	> 0.5	Sustainability and slight decrease	21.85
$\beta \geq 0$	$ Z < 1.96$	> 0.5	Sustainability and slight increase	34.69
$\beta \geq 0$	$ Z \geq 1.96$	> 0.5	Sustainability and significant increase	34.65
--	--	< 0.5	Undetermined future variation trend	2.90

of the vegetation LAI is difficult to determine represented only 2.9% of the total area of global vegetation coverage, which is scattered across the globe. The continuous degradation and vegetation status of the uncertain areas need further investigation.

Vegetation drivers

Fig. 10 shows the spatial distributions of the LAI sensitivities to the driving factors from 1982 to 2018. The LAI is highly sensitive to Evap and Pre, and the spatial distributions of the LAI sensitivities to Evap and Pre are similar, while the spatial distributions of the LAI sensitivities to Temp and SoilTemp are similar. The phenomenon that the areas with high sensitivity of global vegetation LAI to Evap and Pre are mainly concentrated in the BW and BS climatic zones is related to the long-term arid environment of these climatic zones. The areas with high sensitivities of the LAI to Temp and SoilTemp were mainly concentrated in the Df and Dw climatic zones, and this phenomenon is related to the long-term low-temperature environments in these climatic zones. These results indicate that vegetation

changes are sensitive to Evap and Pre in arid climate zones and to Temp and SoilTemp in cold climate zones. However, the sensitivity of the LAI to Qair and SoilMoi is low in most regions of the world.

The mean statistics of the LAI to the driving factor sensitivity rates for different climate zones globally from 1982 to 2018 are shown in Table 1. Pre is the most sensitive driver of the LAI in the Af, Am, Aw, Cs, and Cw climate zones. Evap is the most sensitive driver of the LAI in the BS, Cf, Ds, Dw, Df, and Bw climate zones. These results indicate that the vegetation changes in tropical and arid climate regions are most sensitive to Pre, and the vegetation changes in other climate regions are most sensitive to Evap. The sensitivity of the LAI to Qair is higher than that of Evap and Pre in the ET climate zone, which indicates that vegetation changes are more sensitive to temperature changes in the tundra climate zone. The highest sensitivities of the vegetation LAIs to Evap, Temp, Pre, Qair, SoilMoi, and SoilTemp were 0.422 ± 1.369 , 0.11 ± 0.281 , 0.46 ± 0.445 , 0.168 ± 0.232 , 0.082 ± 0.148 and 0.13 ± 0.208 in 14 global climate zones, respectively.

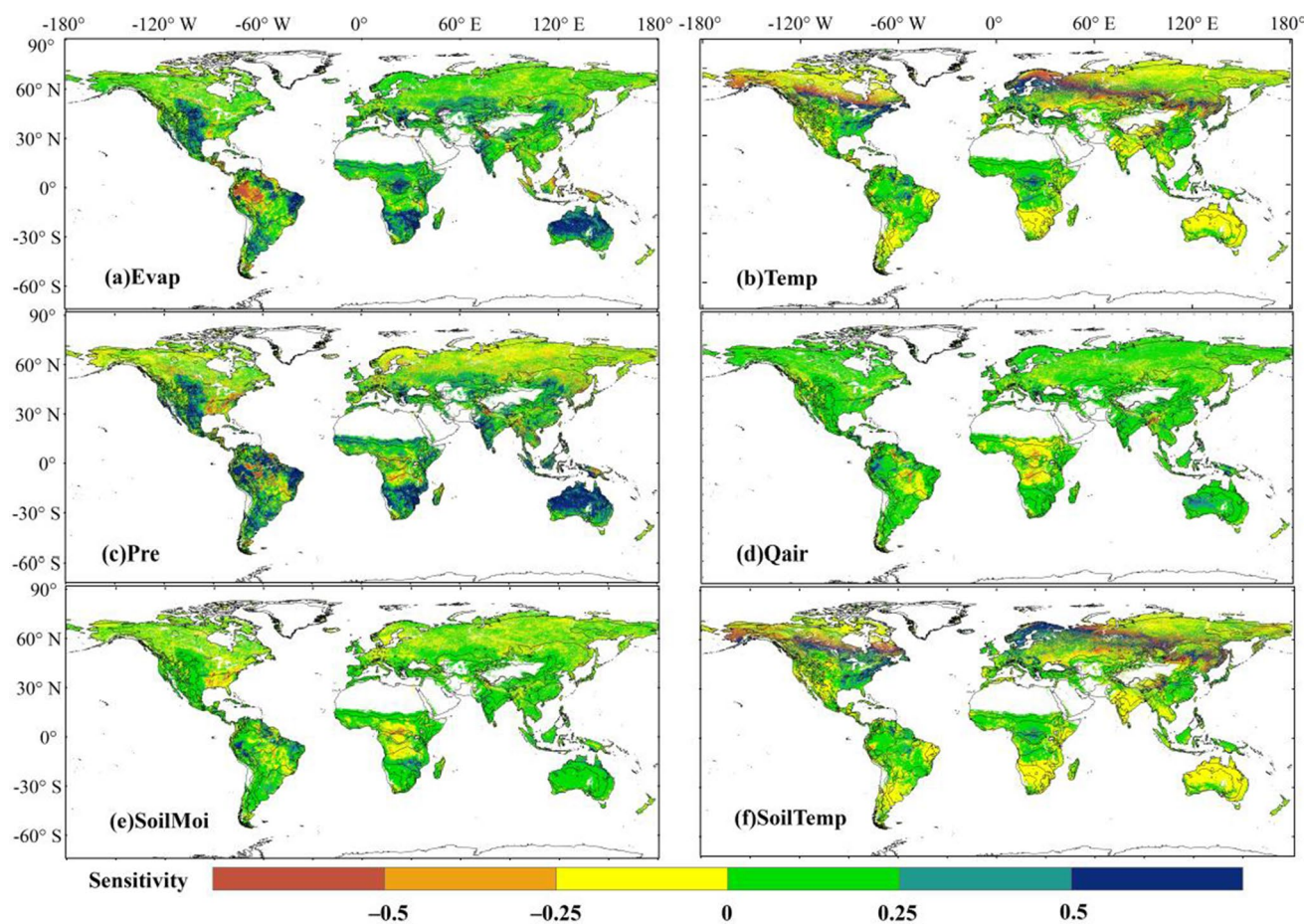


Fig. 10 Spatial distributions of the vegetation LAI sensitivities to the driving factors from 1982 to 2018, (a) Evap, (b) Temp, (c) Pre, (d) Qair, (e) SoilMoi, (f) SoilTemp

Table 1 The mean statistics of the LAIs to the driving factor sensitivity rates for different climate zones globally from 1982 to 2018

GCC	Evap	SoilMoi	Pre	Qair	SoilTemp	Temp
Af	-0.163 ± 0.794	0.11 ± 0.281	0.429 ± 1.044	0.168 ± 0.232	0.056 ± 0.117	0.077 ± 0.15
Am	0.092 ± 0.705	0.067 ± 0.258	0.246 ± 0.796	0.051 ± 0.222	0.082 ± 0.148	0.13 ± 0.208
Aw	0.184 ± 0.419	0.067 ± 0.192	0.221 ± 0.5	0.017 ± 0.163	0.029 ± 0.116	0.052 ± 0.143
BW	0.422 ± 1.369	0.071 ± 0.064	0.46 ± 0.445	0.121 ± 0.124	-0.019 ± 0.368	-0.014 ± 0.42
BS	0.365 ± 2.408	0.086 ± 0.086	0.339 ± 0.314	0.083 ± 0.085	-0.026 ± 0.756	-0.021 ± 0.94
Cs	0.146 ± 0.755	0.056 ± 0.085	0.183 ± 0.33	0.066 ± 0.094	0.026 ± 0.274	0.026 ± 0.287
Cw	0.158 ± 0.284	0.066 ± 0.153	0.195 ± 0.413	0.048 ± 0.173	0.016 ± 0.431	0.034 ± 0.353
Cf	0.127 ± 0.277	0.037 ± 0.16	0.124 ± 0.382	0.079 ± 0.111	0.075 ± 0.285	0.082 ± 0.309
Ds	0.087 ± 0.172	0.02 ± 0.069	0.043 ± 0.217	0.047 ± 0.076	-0.097 ± 1.71	-0.033 ± 1.604
Dw	0.11 ± 0.236	0.016 ± 0.113	0.045 ± 0.31	0.049 ± 0.104	0.007 ± 3.406	0.019 ± 3.165
Df	0.069 ± 0.285	0.002 ± 0.095	-0.017 ± 0.226	0.052 ± 0.086	0.044 ± 2.648	-0.049 ± 2.843
ET	0.01 ± 0.076	0.004 ± 0.059	-0.029 ± 0.109	0.044 ± 0.061	-0.07 ± 0.701	-0.05 ± 0.595
EF	0.166 ± 0.246	0.042 ± 0.078	0.049 ± 0.185	0.113 ± 0.156	0.066 ± 0.183	0.068 ± 0.207
Bw	0.163 ± 0.144	0.031 ± 0.038	0.153 ± 0.173	0.094 ± 0.08	-0.119 ± 1.885	-0.138 ± 0.959

The spatial distributions of the contribution rates of the driving factors to the vegetation LAIs from 1982 to 2018 are shown in Fig. 11. The spatial distributions of the Evap and

Pre contributions to the LAI are similar, while the spatial distributions of the Temp and SoilTemp contributions to the LAI are similar. SoilMoi has the highest contribution rate

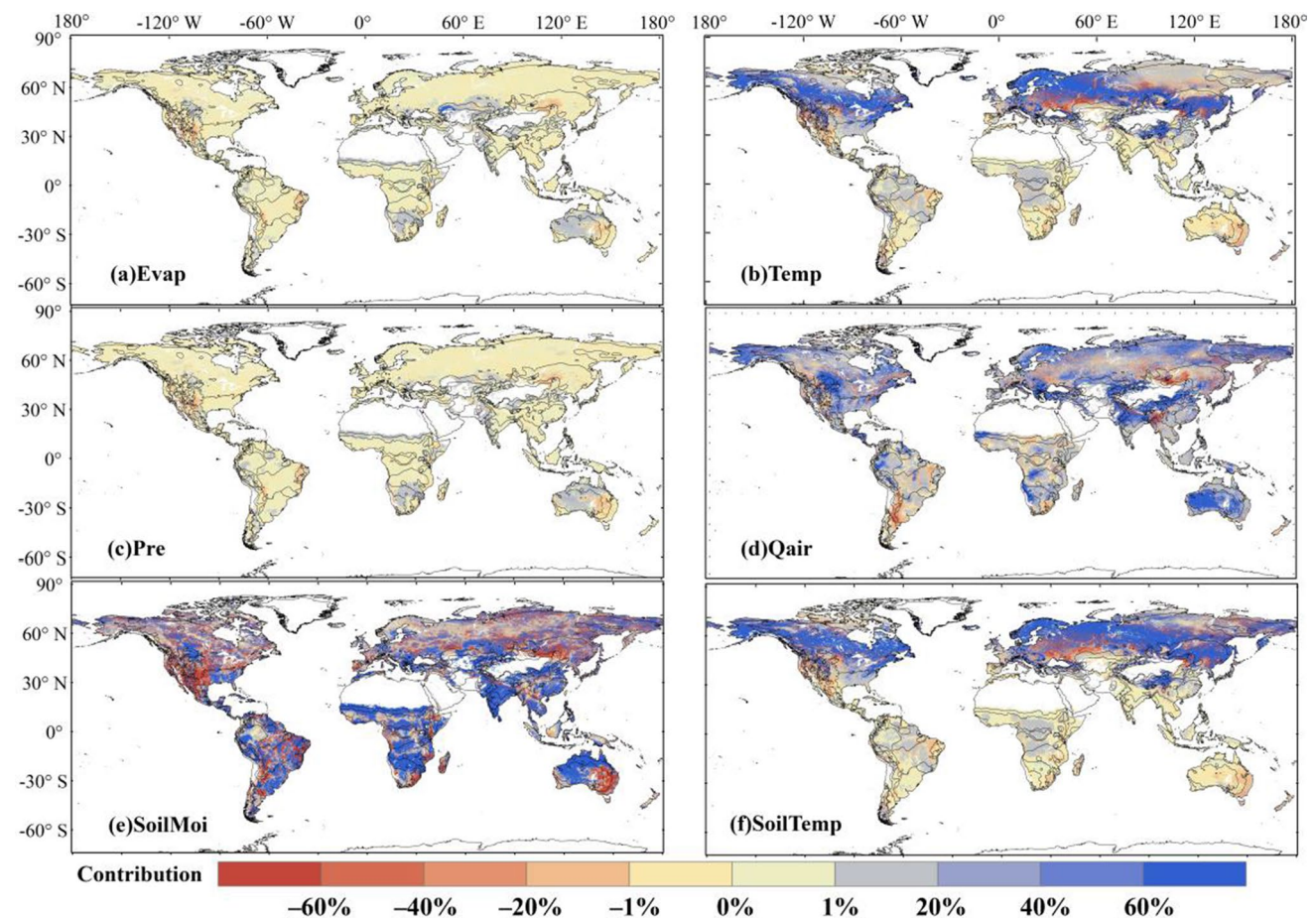


Fig. 11 Spatial distributions of the contribution rates of the driving factors to the vegetation LAI from 1982 to 2018, (a) Evap, (b) Temp, (c) Pre, (d) Qair, (e) SoilMoi, (f) SoilTemp

to the LAI, with an area that contributes more than 60% in absolute terms accounting for 50.26% of the total area of global vegetation cover, which indicates the importance of SoilMoi to vegetation growth and development. The regions with high contribution rates of Temp and SoilTemp to the LAI are mainly distributed in the Northern Hemisphere, which indicates that the highest contributions from temperature to vegetation change were observed in low-temperature environments. The regions with high contribution rates of Qair to the LAI are distributed in central North America, Western and Eastern Europe, Central and Southeast Asia, and Western Australia. Relatively speaking, the contribution rates of Evap and Pre to the LAI are generally low.

Statistics of the average contribution rate of the driving factors of different climate zones in the global to the vegetation LAI from 1982 to 2018 (Table 2). Among the Af, Am, Aw, BW, BS, Cs, Cw, Cf, and EF climate zones, SoilMoi has the highest contribution rate to the vegetation LAI. Among the Ds, Dw, Df, ET, and Bw climate zones, SoilTemp has the highest contribution rate to the vegetation LAI. These results indicate that SoilTemp has the highest contribution to vegetation change in cold climate zones, SoilMoi has the highest contribution to vegetation change in the other climate zones, and soil environmental conditions have the highest contribution to vegetation change. Among the 14 climate zones globally, the highest contribution rates of Evap, Temp, Pre, Qair, SoilMoi, and SoilTemp to vegetation change were 8.42 ± 60.79 , 157.29 ± 206.37 , 2.79 ± 14.4 , 192.79 ± 163.53 , 213.74 ± 227.07 , and 166.34 ± 253.59 , respectively.

Geodetector analysis

The influence of global and different climate zone drivers on LAI changes (Table 3). Globally, the driving factors

affecting LAI changes are Qair, Temp, SoilTemp, Evap, Pre, and SoilMoi in descending order. The driving factors affecting LAI changes varied among climate zones, with Pre being the main influence factor for Aw, Cf, Ds, Df, and Bw climate zones. Qair is the main influence factor for BW, BS, and Cs climate zones, and SoilTemp is the main influence factor for Af, Cw, and Dw climate zones. In addition, SoilMoi and Temp are the main influencing factors for Am and ET climate zones, respectively.

Figure 12 shows the interaction test of the effects of global and different climate zone drivers on LAI changes. As shown in Table 3 and Figure 12, the combined contribution of the driving factors is significantly higher than that of a single factor. On the global scale, $Qair \cap SoilMoi$ has the strongest influence on LAI change, and this phenomenon also occurs in BS, Cs, and Cw climate zones. Meanwhile, in Ds, Df, and Bw climate zones, LAI changes are mainly influenced by $Evap \cap Pre$. A comprehensive analysis of the effects of global and two-factor interactions on LAI changes in different climate zones shows that LAI changes are mainly influenced by $Evap \cap Pre$, followed by $Pre \cap Temp$, and $SoilTemp \cap Temp$ has the weakest effect on LAI changes.

Discussion

Vegetation changes and driving factors

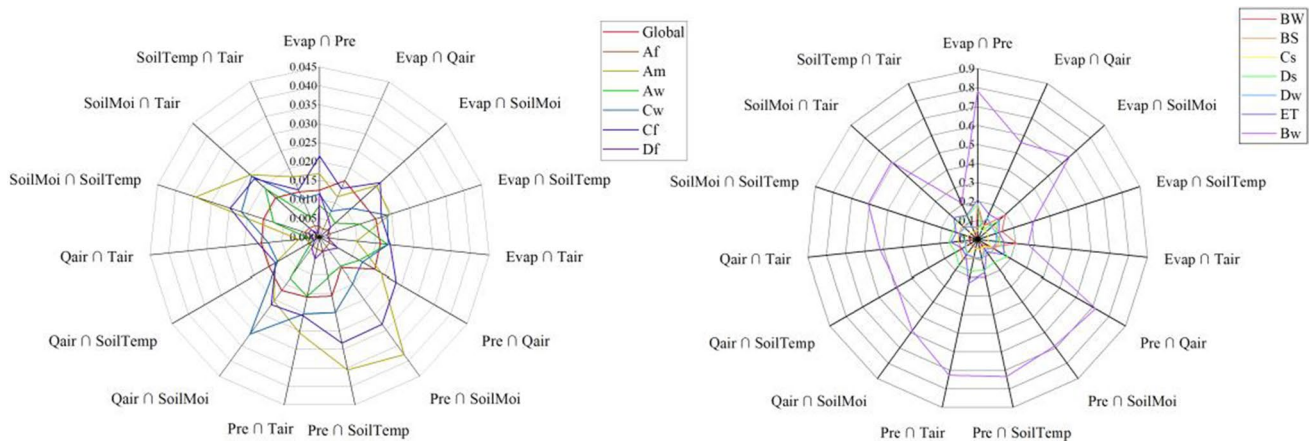
The global vegetation cover is also changing rapidly due to global change, which thus affects ecosystem functions and services (Zhu et al. 2016). The high-value regions of the global vegetation LAI described in “Average LAI of global vegetation” are mainly distributed in northern South America, central Africa, and southeastern Asia,

Table 2 Statistics of the average values of the contribution rates of the driving factors of different climate zones to the vegetation LAI

GCC	Evap	SoilMoi	Pre	Qair	SoilTemp	Temp
Af	0.74 ± 15.35	63.26 ± 152.46	0.45 ± 1.81	19.29 ± 36.33	1.01 ± 4.64	1.81 ± 9.34
Am	0.91 ± 19.91	73.71 ± 184.39	0.21 ± 0.67	7.16 ± 39.75	1.64 ± 4.61	3.37 ± 11.21
Aw	0.42 ± 13.35	116.75 ± 221.13	0.16 ± 0.78	8.13 ± 26.19	0.94 ± 3.73	1.72 ± 8.78
BW	5.15 ± 35.39	91.79 ± 165.94	2.79 ± 14.4	51.96 ± 77.77	4.95 ± 59.16	5.16 ± 63.2
BS	8.42 ± 60.79	99.99 ± 214.67	0.86 ± 3.07	32.09 ± 63.21	20.73 ± 110.92	25.64 ± 116.65
Cs	2.08 ± 31.12	34.89 ± 155.79	0.11 ± 1.94	25.38 ± 48.83	7.27 ± 50.77	8.86 ± 54.43
Cw	0.23 ± 2.95	110.13 ± 205.59	0.27 ± 0.84	14.14 ± 62.12	9.01 ± 64.67	10.08 ± 64.7
Cf	0.32 ± 9.8	68.88 ± 189.88	0.13 ± 1.11	15.48 ± 37.47	12.75 ± 57	12.48 ± 56.97
Ds	0.5 ± 2.38	38.77 ± 150.01	0.27 ± 1.47	37.5 ± 66.67	163.08 ± 245.33	127.7 ± 215.15
Dw	0.08 ± 2.41	37.26 ± 190.1	0.09 ± 1.06	29.08 ± 91.52	207.58 ± 269.37	166.34 ± 253.59
Df	0.25 ± 5.94	28.1 ± 149.67	0.09 ± 0.51	30.93 ± 54.7	201.7 ± 254.83	154.78 ± 234.45
ET	0.06 ± 0.49	40.4 ± 165.8	0.05 ± 0.33	43.2 ± 76.8	48.63 ± 129.32	21.49 ± 82
EF	0.66 ± 1.04	157.29 ± 206.37	0.11 ± 0.43	110.85 ± 125.55	60.52 ± 123.18	46.5 ± 95.42
Bw	2.55 ± 3.82	104.78 ± 120.47	1.48 ± 1.86	192.79 ± 163.53	213.74 ± 227.07	145.18 ± 196.5

Table 3 Effects of global and different climate zone drivers on LAI changes

	GCC	Evap	Pre	Qair	SoilMoi	SoilTemp	Temp
Global		0.0107	0.0052	0.0146	0.0013	0.0124	0.0128
Af		0.0000	0.0006	0.0000	0.0004	0.0007	0.0003
Am		0.0011	0.0119	0.0018	0.0130	0.0109	0.0025
Aw		0.0040	0.0069	0.0009	0.0026	0.0001	0.0005
BW		0.0121	0.0224	0.0320	0.0009	0.0198	0.0175
BS		0.0619	0.0219	0.0893	0.0055	0.0607	0.0621
Cs		0.0253	0.0090	0.0664	0.0075	0.0388	0.0375
Cw		0.0016	0.0048	0.0022	0.0036	0.0081	0.0075
Cf		0.0097	0.0118	0.0073	0.0060	0.0078	0.0080
Ds		0.0065	0.1103	0.0376	0.1058	0.0810	0.0996
Dw		0.0166	0.0236	0.0318	0.0147	0.0621	0.0601
Df		0.0011	0.0024	0.0004	0.0020	0.0002	0.0001
ET		0.1102	0.0385	0.0824	0.0233	0.0751	0.1361
Bw		0.2118	0.6216	0.4487	0.5523	0.1771	0.0724

**Fig. 12** Interaction detection of the effects of global and different climate zone drivers on LAI changes

which are basically consistent with the results of previous studies on the spatial distributions of the global vegetation LAI (Liu et al. 2010; Zhu et al. 2016). The vegetation distributions respond to climatic, natural, geographic, and anthropogenic factors, which result in significant differences in the global spatial trends of vegetation cover. In “Global vegetation spatial change” of this study, the area percentage with an increasing trend of global vegetation is generally consistent with the results of Li and Qu (2019). Liu et al. (2013) analyzed the spatiotemporal distributions of the coefficients of variation for the NDVI for global vegetation from 1982 to 2006, which showed relatively low CV values in most areas, which are somewhat different from the findings of this paper that the area was dominated by medium-high fluctuations in vegetation, and these differences in the NDVI and LAI analyses were confirmed in the literature results reported by Yuan et al. (2021). The

above analysis shows that the results from this study are generally consistent with those of previous studies.

Land use change, climate change, and biogeochemistry have long-term effects on global vegetation changes (Wang et al. 2014). However, the mutual influence between the driving factors and vegetation change trends causes the responses of vegetation changes in different regions to the driving factors to be different (Liang et al. 2020, Niu et al. 2019). For example, in ecologically fragile areas, precipitation and temperature are the main factors that affect vegetation growth (Hu et al. 2021). In humid regions, the contribution rate of vegetation change to soil moisture is – 40.21% (Feng 2016). In evergreen broad-leaved forests and the tropical savannas in Africa, vegetation growth is most sensitive to precipitation and temperature (Li et al. 2019). However, for all vegetation types, there is a lag of more than 1 month for the influence of radiation on global

vegetation growth. This was also the starting point for this article to study the sensitivities and contributions among vegetation and the influencing factors from 14 climate zones around the world. In addition, previous studies focused more on the spatiotemporal variation of vegetation in the entire study area and its correlation with climatic factors, but they did not quantitatively analyze the spatiotemporal variation and driving factors of vegetation in different climatic subregions. Therefore, this study is important for a comprehensive analysis of the spatiotemporal variation of vegetation and its drivers in different climatic zones.

In addition, some scholars have also studied the sensitivity rates of climate factors to global vegetation by using different methods. For example, Chen et al. (2021) used long short-term memory to study the sensitivity of the NDVI to temperature and precipitation and showed that the NDVI is highly sensitive to temperature in the Northern Hemisphere, while it is highly sensitive to precipitation in the Southern Hemisphere. Yuan et al. (2021) used principal component regression to study the sensitivity rate of vegetation change to temperature and showed that most of the areas with high-temperature sensitivity rates of vegetation change were distributed in the Northern Hemisphere. Quetin and Swann (2017) used least squares regression to analyze the sensitivity of the NDVI to precipitation and showed that the sensitivity of vegetation to precipitation in the Northern Hemisphere is mainly negative, and the sensitivity of vegetation to precipitation in the Southern Hemisphere is mainly positive. By summarizing the above research results, we can see that their research results are more consistent with the analysis results shown in Figure 10 of this paper. In addition, when studying the drivers of vegetation change, we more comprehensively quantified the sensitivity of vegetation change to climate factors and the contribution of climate factors to vegetation change in different climate zones.

It can be seen that the LAI has the highest sensitivity rate to Evap and Pre, but the contribution rate of Evap and Pre to the LAI is very low. SoilMoi has the highest contribution rate to the LAI, but the LAI sensitivity rate to SoilMoi is not the highest. This phenomenon shows that vegetation change is not positively correlated with the sensitivity rates or contribution rates of the driving factors, and this phenomenon is also reported in Sun et al. (2021).

Shortcomings and prospects

This paper comprehensively analyzes the vegetation driving factors and their changes in 14 different climate regions around the world from 1981 to 2018, but there are still some shortcomings. First, the remote sensing inversion product data used in this paper may have accuracy limitations and uncertainties due to factors such as land cover types and raster accuracy sizes (Guli-Jiapaer et al. 2015). Therefore,

in future research, we can use remote sensing data products with higher precision to produce more accurate analysis results. Second, in this paper, only the six drivers of vegetation change were used for the analysis; however, vegetation change also has some responses to other influencing factors. For example, factors such as CO₂ fertilization (Piao et al. 2013), radiation (Piao et al. 2013), and anthropogenic (Chen et al. 2020) can also have impacts on vegetation change. Therefore, comprehensive consideration of the impacts of the driving factors on vegetation changes still needs further improvement. Third, this paper analyzes the impact of 6 influencing factors in different climate zones on the vegetation changes by using the Köppen Global Climate Classification. However, for the same climate zone, whether the responses of different continental vegetation changes to the driving factors are consistent is a question that needs to be considered in future research.

Conclusions

This paper examines the vegetation drivers and their changes in 14 different climatic zones across the globe from 1981 to 2018. The results show that (1) the global vegetation LAI is dominated by an increasing and then decreasing trend, which accounts for approximately 38.61% of the total global vegetation cover area. The global vegetation LAI increased linearly from 1981 to 2018 ($2.88 \times 10^{-3} \text{ year}^{-1}$) and was greater than the nonlinear growth trend ($1.91 \times 10^{-3} \text{ year}^{-1}$). (2) The global vegetation LAI is dominated by medium-high fluctuations and sustainable increasing changes, which account for 61.27% and 69.34% of the total area of global vegetation cover, respectively. The annual average values of the LAI in different ecosystems, from large to small, are EBF, DBF, MFO, ENF, WSA, SAV, DNF, CNM, CRO, PWE, CSH, GRA, and OSH. (3) The sensitivity rates of global vegetation change to Evap and Pre are high, and vegetation change is most sensitive to Pre in tropical and arid climate zones and to Evap in the other climate zones. (4) SoilMoi had the highest contribution rate to vegetation change, the areas with absolute values of contribution rates over 60% accounted for 50.26% of the total global vegetation cover, and the temperature had a high contribution to vegetation change in low-temperature climate zones. (5) Globally, the driving factors influencing LAI changes are Qair, Temp, SoilTemp, Evap, Pre, and SoilMoi in descending order, with the largest interaction effect of Qair and SoilMoi on LAI changes.

Acknowledgements We would like to acknowledge the data support provided by the National Earth System Science Data Center at the National Science & Technology Infrastructure of China (<http://www.geodata.cn>). The data used in this study were acquired as part of the mission of NASA's Earth Science Division and archived and

distributed by the Goddard Earth Sciences (GES) Data and Information Services Center (DISC).

Author contribution Guangchao Li: software, validation, data curation, writing-original draft preparation. Wei Chen: conceptualization, methodology, software, investigation, writing-original draft preparation, writing-reviewing and editing, supervision. Xuepeng Zhang: formal analysis, visualization, investigation, validation. Pengshuai Bi: formal analysis, investigation, validation. Zhen Yang: writing-reviewing and editing. Zhe Wang: software, investigation.

Funding This study was supported by the Beijing Natural Science Foundation (8192037), National Natural Science Foundation of China (41701391), and Fundamental Research Funds for the Central Universities (2014QD02).

Data availability The datasets used and/or analyzed during the current study are available from the corresponding author on reasonable request.

Declarations

Ethics approval and consent to participate Not applicable.

Consent for publication Not applicable.

Competing interests The authors declare no competing interests.

References

- Birhanu D, Kim H, Jang C (2019) Effectiveness of introducing crop coefficient and leaf area index to enhance evapotranspiration simulations in hydrologic models. *Hydrol Processes* 33(16):2206–2226
- Chen C, Park T, Wang X, Piao S, Xu B, Chaturvedi RK, Fuchs R, Brovkin V, Ciais P, Fensholt R, Tommervik H, Bala G, Zhu Z, Nemani RR, Myneni RB (2019) China and India lead in greening of the world through land-use management. *Nat Sustain* 2:122–129
- Chen M, Melaas EK, Gray JM, Friedl MA, Richardson AD (2016) A new seasonal-deciduous spring phenology submodel in the Community Land Model 4.5: impacts on carbon and water cycling under future climate scenarios. *Glob. Change Biol.* 22(11):3675–3688
- Chen Y, Chen L, Cheng Y, Ju W, Chen HYH, Ruan H (2020) Afforestation promotes the enhancement of forest LAI and NPP in China. *Forest Ecol Manage* 462:117990
- Chen Z, Liu H, Xu C, Wu X, Liang B, Cao J, Chen D (2021) Modeling vegetation greenness and its climate sensitivity with deep-learning technology. *Ecol Evol* 11(12):7335–7345
- Deng Y, Wang XH, Wang K, Ciais P, Tang SC, Jin L, Li LL, Piao SL (2021) Responses of vegetation greenness and carbon cycle to extreme droughts in China. *Agri Forest Meteorol* 298:9
- Feng HH (2016) Individual contributions of climate and vegetation change to soil moisture trends across multiple spatial scales. *Scientific Reports* 6:32782
- Gao J, Jiao K, Wu S (2019) Investigating the spatially heterogeneous relationships between climate factors and NDVI in China during 1982 to 2013. *J Geog Sci* 29(10):1597–1609
- Ge J, Guo W, Pitman AJ, De Kauwe MG, Chen X, Fu C (2019) The nonradiative effect dominates local surface temperature change caused by afforestation in China. *J Climate* 32(14):4445–4471
- Guli-Jiapaer, Liang S, Yi Q, Liu J (2015) Vegetation dynamics and responses to recent climate change in Xinjiang using leaf area index as an indicator. *Ecol Ind* 58:64–76
- Hu Y, Li H, Wu D, Chen W, Zhao X, Hou M, Li A, Zhu Y (2021) LAI-indicated vegetation dynamic in ecologically fragile region: a case study in the Three-North Shelter Forest program region of China. *Ecol Ind* 120:106932
- Hu ZM, Yu GR, Fu YL, Sun XM, Li YN, Shi PL, Wang YF, Zheng ZM (2008) Effects of vegetation control on ecosystem water use efficiency within and among four grassland ecosystems in China. *Glob. Change Biol.* 14(7):1609–1619
- Huang NE, Shen Z, Long SR, Wu MC, Shin HH, Zheng Q, Nai-Chyuan Y, Chao TC, H LH (1998) The empirical mode decomposition and the Hilbert spectrum for nonlinear and non-stationary time series analysis. *Proc. R. Soc. Lond. A* 454: 903–995
- Jin Z, Liang W, Yang Y, Zhang W, Yan J, Chen X, Li S, Mo X (2017) Separating vegetation greening and climate change controls on evapotranspiration trend over the Loess Plateau. *Sci Rep* 7(1):8191
- Kahiu MN, Hanan NP (2018) Estimation of woody and herbaceous leaf area index in sub-Saharan Africa using MODIS data. *J. Geophys. Res.-Biogeosci.* 123(1):3–17
- Kottek M, Grieser J, Beck C, Rudolf B, Rubel F (2006) World map of the Köppen-Geiger climate classification updated. *Meteorologische Zeitschrift* 15(3):259–263
- Li GC, Chen W, Li RR, Zhang XP, Liu JL (2021) Assessing the spatiotemporal dynamics of ecosystem water use efficiency across China and the response to natural and human activities. *Ecol Ind* 126:107680
- Li W, Du J, Li S, Zhou X, Duan Z, Li R, Wu S, Wang S, Li M (2019) The variation of vegetation productivity and its relationship to temperature and precipitation based on the GLASS-LAI of different African ecosystems from 1982 to 2013. *Int J Biometeorol* 63(7):847–860
- Li X, Qu Y (2019) Evaluation of vegetation responses to climatic factors and global vegetation trends using GLASS LAI from 1982 to 2010. *Canadian J Remote Sens* 44(4):357–372
- Li Y, Shi H, Zhou L, Eamus D, Huete A, Li LH, Cleverly J, Hu ZM, Harahap M, Yu Q, He L, Wang SQ (2018) Disentangling climate and LAI effects on seasonal variability in water use efficiency across terrestrial ecosystems in China. *J. Geophys. Res.-Biogeosci.* 123(8):2429–2443
- Liang B, Liu H, Chen X, Zhu X, Cressey EL, Quine TA (2020) Periodic relations between terrestrial vegetation and climate factors across the globe. *Remote Sens* 12(11):1805
- Liu G, Liu H, Yin Y (2013) Global patterns of NDVI-indicated vegetation extremes and their sensitivity to climate extremes. *Environ Res Lett* 8(2):025009
- Liu H, Zhang M, Lin Z, Xu X (2018) Spatial heterogeneity of the relationship between vegetation dynamics and climate change and their driving forces at multiple time scales in Southwest China. *Agri Forest Meteorol* 256–257:10–21
- Liu S, Liu R, Liu Y (2010) Spatial and temporal variation of global LAI during 1981–2006. *J Geog Sci* 20(3):323–332
- Liu Y, Ju W, Chen J, Zhu G, Xing B, Zhu J, He M (2012) Spatial and temporal variations of forest LAI in China during 2000–2010. *Chinese Sci Bull* 57(22):2846–2856
- Liu Y, Li Y, Li SC, Motesharrei S (2015) Spatial and temporal patterns of global NDVI trends: correlations with climate and human factors. *Remote Sensing* 7(10):13233–13250
- McNally A, Arsenault K, Kumar S, Shukla S, Peterson P, Wang SG, Funk C, Peters-Lidard CD, Verdin JP (2017) Data descriptor: a land data assimilation system for sub-Saharan Africa food and water security applications. *Scientific Data* 4:170012
- Niu Z, He H, Zhu G, Ren X, Zhang L, Zhang K, Yu G, Ge R, Li P, Zeng N, Zhu X (2019) An increasing trend in the ratio of transpiration to total terrestrial evapotranspiration in China from 1982

- to 2015 caused by greening and warming. *Agri Forest Meteorol* 279:107701
- Pascolini-Campbell M, Reager JT, Chandanpurkar HA, Rodell M (2021) A 10 per cent increase in global land evapotranspiration from 2003 to 2019. *Nature* 593(7860):543–547
- Piao S, Yin G, Tan J, Cheng L, Huang M, Li Y, Liu R, Mao J, Myneni RB, Peng S, Poulter B, Shi X, Xiao Z, Zeng N, Zeng Z, Wang Y (2015) Detection and attribution of vegetation greening trend in China over the last 30 years. *Glob Chang Biol* 21(4):1601–1609
- Piao SL et al (2013) Evaluation of terrestrial carbon cycle models for their response to climate variability and to CO₂ trends. *Glob. Change Biol.* 19(7):2117–2132
- Quetin GR, Swann ALS (2017) Empirically derived sensitivity of vegetation to climate across global gradients of temperature and precipitation. *J Climate* 30(15):5835–5849
- Sprintsin M, Karnieli A, Berliner P, Rotenberg E, Yakir D, Cohen S (2007) The effect of spatial resolution on the accuracy of leaf area index estimation for a forest planted in the desert transition zone. *Remote Sens Environ* 109(4):416–428
- Sun H, Bai Y, Lu M, Wang J, Tuo Y, Yan D, Zhang W (2021) Drivers of the water use efficiency changes in China during 1982–2015. *Sci Total Environ* 799:149145
- Wang JF, Zhang TL, Fu BJ (2016) A measure of spatial stratified heterogeneity. *Ecol Ind* 67:250–256
- Wang XH, Piao SL, Ciais P, Friedlingstein P, Myneni RB, Cox P, Heimann M, Miller J, Peng SS, Wang T, Yang H, Chen AP (2014) A two-fold increase of carbon cycle sensitivity to tropical temperature variations. *Nature* 506(7487):212–+
- Xiao JF, Moody A (2004) Trends in vegetation activity and their climatic correlates: China 1982 to 1998. *Intl J Remote Sens* 25(24):5669–5689
- Xiao Z, Liang S, Wang J, Chen P, Yin X, Zhang L, Song J (2014) Use of general regression neural networks for generating the GLASS leaf area index product from time-series MODIS surface reflectance. *Ieee Trans Geosci Remote Sens* 52(1):209–223
- Xiao Z, Liang S, Wang T, Jiang B (2016) Retrieval of leaf area index (LAI) and fraction of absorbed photosynthetically active radiation (FAPAR) from VIIRS time-series data. *Remote Sensing* 8(4):351
- Yin Y, Wu S, Dai E (2010) Determining factors in potential evapotranspiration changes over China in the period 1971–2008. *Chinese Sci Bull* 55(29):3329–3337
- Yin Y, Ma D, Wu S, Dai E, Zhu Z, Myneni RB (2017) Nonlinear variations of forest leaf area index over China during 1982–2010 based on EEMD method. *Int J Biometeorol* 61(6):977–988
- Yuan X, Hamdi R, Ochege FU, Kurban A, De Maeyer P (2021) The sensitivity of global surface air temperature to vegetation greenness. *Intl J Climatol* 41(1):483–496
- Zeng Z, Piao S, Li LZX, Zhou L, Ciais P, Wang T, Li Y, Lian X, Wood EF, Friedlingstein P, Mao J, Estes LD, Myneni Ranga B, Peng S, Shi X, Seneviratne SI, Wang Y (2017) Climate mitigation from vegetation biophysical feedbacks during the past three decades. *Nature Climate Change* 7(6):432–436
- Zhang JT, Zhang YQ, Qin SG, Wu B, Wu XQ, Zhu YK, Shao YY, Gao Y, Jin QT, Lai ZR (2018) Effects of seasonal variability of climatic factors on vegetation coverage across drylands in northern China. *Land Degradation & Development* 29(6):1782–1791
- Zhang QA, Chen W (2021) Ecosystem water use efficiency in the Three-North Region of China based on long-term satellite data. *Sustainability* 13(14):7977
- Zhang ZY, Wong MS, Nichol J (2016) Global trends of aerosol optical thickness using the ensemble empirical mode decomposition method. *Intl J Climatol* 36(13):4358–4372
- Zheng HX, Zhang L, Zhu RR, Liu CM, Sato Y, Fukushima Y (2009) Responses of streamflow to climate and land surface change in the headwaters of the Yellow River Basin. *Water Resources Research* 45:W00A19
- Zhu L, Chen JM, Tang S, Li G, Guo Z (2014) Inter-comparison and validation of the FY-3A/MERSI LAI product over Mainland China. *IEEE J Select Top Appl Earth Observ Remote Sens* 7(2):458–468
- Zhu ZC et al (2016) Greening of the Earth and its drivers. *Nature Climate Change* 6(8):791–+

Publisher's note Springer Nature remains neutral with regard to jurisdictional claims in published maps and institutional affiliations.